

Atomic excitation delocalization at the clean to disordered interface in a chirally-coupled atomic array

C.-C. Wu,^{1,*} K.-T. Lin,² I. G. N. Y. Handayana,^{1,3,4} C.-H. Chien,^{1,2}

S. Goswami,¹ G.-D. Lin,^{2,5,6} Y.-C. Chen¹ and H. H. Jen^{1,5*}

¹*Institute of Atomic and Molecular Sciences, Academia Sinica, Taipei 10617, Taiwan*

²*Department of Physics and Center for Quantum Science and Engineering,
National Taiwan University, Taipei 10617, Taiwan*

³*Molecular Science and Technology Program, Taiwan International Graduate Program, Academia Sinica, Taiwan*

⁴*Department of Physics, National Central University, Taoyuan City 320317, Taiwan*

⁵*Physics Division, National Center for Theoretical Sciences, Taipei 10617, Taiwan and*

⁶*Trapped-Ion Quantum Computing Laboratory, Hon Hai Research Institute, Taipei 11492, Taiwan*

(Dated: December 15, 2023)

In one-dimensional quantum emitter systems, the dynamics of atomic excitations are influenced by the collective coupling between emitters through photon-mediated dipole-dipole interactions. By introducing positional disorders in a portion of the atomic array, we investigate the delocalization phenomena at the interface between disordered zone and clean zone. The excitation is initialized as symmetric Dicke states in the disordered zone, and several measures are used to quantify the excitation localization. We first use population imbalance and half-chain entropy to investigate the excitation dynamics under time evolutions, and further investigate the crossover of excitation localization to delocalization via the gap ratio from the eigenspectrum in the reciprocal coupling case. In particular, we study the participation ratio of the whole chain and the photon loss ratio between both ends of the atomic chain, which can be used to quantify the delocalization crossover in the non-reciprocal coupling cases. Furthermore, by increasing the overall size or the ratio of the disordered zone under a fixed number of the whole chain, we observe that excitation localization occurs at a smaller disorder strength in the former case, while in the latter, a facilitation of the delocalization appears when a significant ratio of clean zone to disordered zone is applied. Our results can reveal the competition between the clean zone and the disordered zone sizes on localization phenomenon, give insights to non-equilibrium dynamics in the emitter-waveguide interface, and provide potential applications in quantum information processing.

I. INTRODUCTION

Quantum particle dynamics in the random potential of disordered lattices have been extensively studied since Anderson's work on single particle localization [1]. In Anderson's primary work, even though the spin can transport between lattice sites through dipolar interaction, the spin diffusion remains absent when the random energy is introduced from site to site. Besides Anderson localization in a non-interacting regime [2–6], this single particle localization is still signified in an extensive category of closed quantum system even when significant interactions are involved [7–10]. With these unique phenomena, abundant investigations have been explored accordingly, like many-body localization [11, 12] and ergodicity in a closed system [13–15]. Among this research, one of topics that has attracted much interest in quantum dynamics is disordered-induced localization influenced by additional baths [16–21]. Unlike fully disordered systems, once an additional bath interacts with an initially localized system, the localization may break down under the influence of the baths [16, 17, 19–21]. This has led to recent studies on quantum avalanches influenced by the clean

system size [18, 21]. Quantum avalanches represent an accelerated bath penetration into the localization zone as the clean system size increases. In the recent experiment [18], the localization is still robust under the influence of a small-size bath, whereas the localization melts down acceleratedly when coupled to a large-size bath.

Despite rich explorations in localization have been achieved, current research is predominantly on finite range coupling and closed systems. The localization behavior on an intrinsic open system is still less investigated because the inevitable dissipation make the phase transition from localization to delocalization hard to be identified. Until recently, single particle localization and many-body localization have been explored in an open system [22–24]. However, whether an additional bath induces the localization breakdown has also been scarcely explored in an open system, and the influence of an additional bath is still unclear. In this study, we focus on single excitation diffusion in a one-dimensional two-level quantum emitters (TLQE) array coupled to the photonic waveguides [25, 26], via the evanescent waves [27]. In addition to study localization and non-equilibrium dynamics in a closed and finite range coupling system [28, 29], a TLQE array also offers an opportunity to investigate localization in an open and all-to-all interaction system [25, 26, 30–33]. Moreover, many related phenomena have already been explored in one-dimensional equidistant TLQE with chiral couplings, like localization

* Corresponding authors: freddywu0811@gmail.com; sappyjen@gmail.com

[22, 23, 34–37], photon transport [3, 34, 35, 38–42], photon storage [43–46], excitation dynamics [23, 45, 47–49], and photon-mediated localization [50].

In this work, we apply disorders only to a half-chain of the TLQE with chiral couplings [51], creating an interface between the disordered zone and the clean zone. We then investigate the excitation distribution dynamics at long time and determine the crossover of delocalization to disorder-induced localization phases under the influence of clean zones. Additionally, we study photon loss from the TLQE, which serves as a measure of delocalization with initialized symmetric Dicke states in the disordered zone. Furthermore, we examine the influences of system sizes on the phase boundary and on the excitation distributions near the interface. We find that localization is enhanced with a larger ratio of the disordered zone or with a larger overall system size, while increasing the ratio of the clean zone can further delocalize the excitations in the disordered zone when a significant clean zone ratio is applied. Our work explores the modified excitation localization at the clean-disordered interface in a chirally-coupled atomic array, which can provide insights to non-equilibrium quantum dynamics and controlled retention of initialized quantum states in open quantum systems.

The paper is organized as follows. In Sec. II, we introduce the theoretical model for a chirally-coupled one-dimensional atomic chain and describe the system setup. In Sec. III, we compare the clean-disordered system with the fully disordered system by population imbalance and half-chain entropy, and identify the localization in the disordered zone and near the interface. In Sec. IV, we investigate the gap ratios and the participation ratio, both of which can serve as measures for the excitation localization. In Sec. V, we investigate the directional photon loss ratio, providing insights into the excitation dynamics and serving as a measure of the localization crossover. In Sec. VI, we further discuss the influence of the size of the clean and disordered zones on the localization crossover point. In Sec. VII, we summarize the localization properties in the TLQE system and explore the feasibility of photon measurement in different platforms. We also discuss potential future works with similar setups.

II. THEORETICAL MODEL

We consider a general model in Lindblad forms for a periodic 1D quantum emitters coupled to the photonic waveguides with chiral couplings [23, 52], as depicted in Fig. 1. For each two-level emitter, we denote $|e\rangle$ and $|g\rangle$ for the excited and ground states with transition frequency ω_{eg} . Without any field driving, the density matrix ρ of N two-level emitters evolution in the interaction picture is determined by the master equation (See Appendix. A) ($\hbar = 1$)

$$\frac{d\rho}{dt} = -i[H_L + H_R, \rho] + \mathcal{L}_L[\rho] + \mathcal{L}_R[\rho], \quad (1)$$

where the free evolution of the energy difference $\sum_{\mu}^N \omega_{eg} |e\rangle_{\mu} \langle e|$ is absorbed into the excited states as we assume the resonance between two level energy difference and the field that excites the emitters. The coherent parts and dissipative parts in Equation. (1) read

$$H_{L(R)} = -i \frac{\gamma_{L(R)}}{2} \sum_{\mu < (>) \nu} \sum_{\nu=1}^N (e^{ik_s|x_{\mu}-x_{\nu}|} \sigma_{\mu}^{\dagger} \sigma_{\nu} - \text{H.c.}), \quad (2)$$

and

$$\begin{aligned} \mathcal{L}_{L(R)}[\rho] = & -\frac{\gamma_{L(R)}}{2} \sum_{\mu, \nu} e^{\mp ik_s(x_{\mu}-x_{\nu})} (\sigma_{\mu}^{\dagger} \sigma_{\nu} \rho \\ & + \rho \sigma_{\mu}^{\dagger} \sigma_{\nu} - 2\sigma_{\nu} \rho \sigma_{\mu}^{\dagger}) \end{aligned} \quad (3)$$

respectively, where $\sigma_{\mu}^{\dagger} \equiv |e\rangle_{\mu} \langle g|$ with $\sigma_{\mu} = (\sigma_{\mu}^{\dagger})^{\dagger}$ denotes the dipole operator. k_s and $\gamma_{L(R)}$ denote the photon wave vector and the coupling strength to the left(right) of each quantum emitter. Eq. (1) is obtained with Born-Markov approximation [53] under one-dimensional reservoirs, where non-reciprocal and infinite-range photon-mediated dipole-dipole interactions determine the spin-exchange processes [54].

The asymmetric of the coupling strength $\gamma_{L(R)}$ are dependent on the photon propagation direction and the polarization of the transition dipole moment of the quantum emitters [51, 55]. When the light is strongly transversely confined near the surface of the waveguide, the confinement results in a relation between local polarization and the photon propagation direction. Therefore, polarization-dependent coupling of an emitter results in the chiral coupling. Until now, the chiral feature has been achieved on atoms coupling to a nanofiber [56, 57], or a photonic waveguide [58, 59].

A parameter to specify the directionality of couplings $D \equiv \frac{\gamma_R - \gamma_L}{\gamma_R + \gamma_L}$ [59] defines the tendency of effective light transfer. The decay rate $\gamma = \gamma_R + \gamma_L \equiv 2|dq(\omega)/d\omega|_{\omega=\omega_{eg}} g_{k_s}^2 L$ [60], where $|dq(\omega)/d\omega|$ denotes the inverse of group velocity with a resonant wave vector $q(\omega)$, g_{k_s} denotes the coupling strength, and L denotes the quantization length. $D \in [-1, 1]$ specifies the trend of photon exchange between quantum emitters, and when $D = 0$, the system returns to a reciprocal coupling regime. For one-dimensional quantum emitters array with equal interatomic distances, $\xi \equiv k_s|x_{\mu+1} - x_{\mu}|$ is used to specify the photon-mediated dipole-dipole interactions strength which mediates the whole system. An additional significant parameter $W_{\mu} \in \pi[-\bar{w}, \bar{w}]$ is introduced to denote the onsite phase disorders with $\bar{w} \in [0, 1]$. Onsite phase disorders W_{μ} can be established

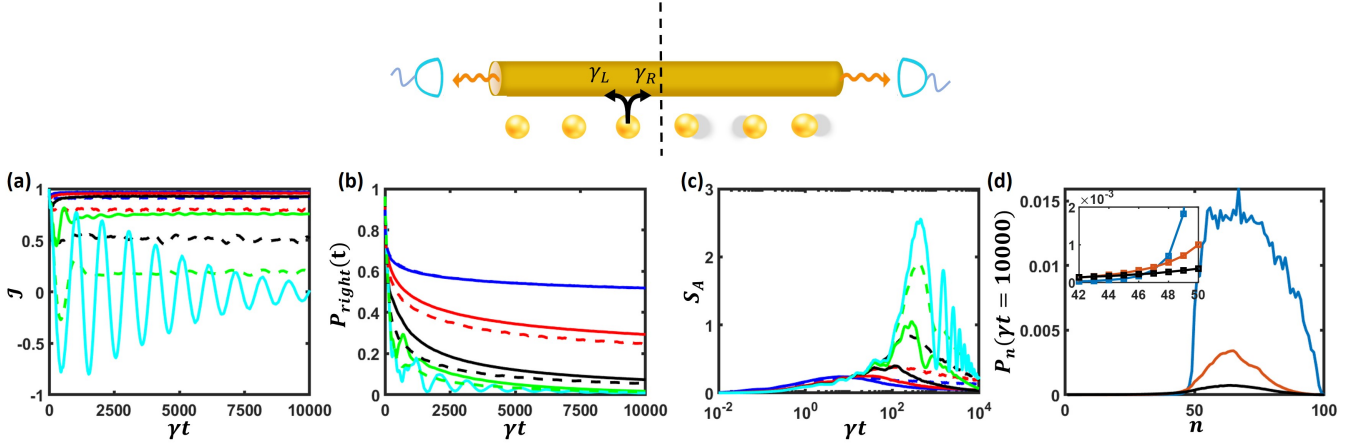


FIG. 1. Schematic plot for an emitter-waveguide interface with chiral couplings (γ_L and γ_R), where the right half-chain is under disorders. The time evolution of (a) imbalance, (b) the excitation population in the right half-chain, and (c) half-chain entropy in logarithmic time scale for $N = 100$, $\xi/\pi = 0.25$, $D = 0.2$, and $\bar{w}/\pi = 0.5, 0.2, 0.1, 0.05, 0$ (blue, red, black, green, and cyan line) in the clean-disordered (fully disordered) system as solid (dash) line. (d) The excitation distribution at $\xi/\pi = 0.25, D = 0.2, \gamma t = 10^4$ for $\bar{w}/\pi = 0.5, 0.1, 0.05$ (blue, red, and black). The inset figure is the excitation distribution near the interface.

in a quantum emitter array from atomic deviated positions, leading to a deviation of ξ in Eqs. (2) and (3).

As shown in Fig. 1, the system is composed of the clean zone and disordered zone. For emitters in the clean zone, there are no onsite atomic deviated positions. Whereas additional position fluctuations are added for emitters in the disordered zone, which causes onsite phase disorders. The system is initialized from a single excitation in the disordered zone. As a consequence, the single excitation subspace composed of $|\psi\rangle_\mu = |e\rangle_\mu |g\rangle^{\otimes(N-1)}$ should be sufficient for describing the system evolution. In this subspace, the excitation state can be written as $|\Psi(t)\rangle = \sum_{\mu=1}^N a_\mu(t) |\psi(t)\rangle$, and the non-Hermitian effective Hamiltonian reads [52, 61],

$$H_{eff} = -i\frac{\gamma_L}{2} \sum_{\mu < \nu} \sum_{\nu=1}^N e^{ik_s|x_\mu - x_\nu|} \sigma_\mu^\dagger \sigma_\nu - i\frac{\gamma_R}{2} \sum_{\mu > \nu} \sum_{\nu=1}^N e^{ik_s|x_\mu - x_\nu|} \sigma_\mu^\dagger \sigma_\nu - i\frac{\gamma}{2} \sum_{\nu=1}^N \sigma_\nu^\dagger \sigma_\nu. \quad (4)$$

Therefore, the state evolution can be reduced to

$$\dot{a}_\mu(t) = \gamma_L \sum_{\mu < \nu} e^{-i(\mu-\nu)\xi - i(W_\mu - W_\nu)} a_\nu(t) - \frac{\gamma}{2} a_\mu(t) - \gamma_R \sum_{\mu > \nu} e^{i(\mu-\nu)\xi - i(W_\nu - W_\mu)} a_\nu(t). \quad (5)$$

In the below, we solve the time dynamics of excitation via Eq. (5) and investigate the influence of the interface on the localization in the disordered zone.

III. LOCALIZATION IN DISORDERED ZONE AND NEAR INTERFACE

First, we would like to clarify the influence of the clean zone in the TLQE system. Consequently, we focus on the localization robustness in the disordered zone and study the excitation dynamics. To make sure the excitation is not influenced by the distance to the interface and the boundary, we consider the symmetric Dicke state in the disordered zone as the initial state. Therefore, we have $a_\mu(0) = 0$ and vanishing phase disorders W_μ in the clean zone. As a comparison, we use a fully disordered TLQE system initialized with the symmetric Dicke state that $a_\mu = 1/\sqrt{N/2}$ for $\mu \in [\frac{N}{2} + 1, N]$ and investigate the effect of the clean zone on the excitation delocalization.

As time evolves, the dipole-dipole interaction between emitters transports and dissipates the excitations. To quantify the excitation transport from the right half-chain, we define a time-dependent imbalance

$$\mathcal{J}(t) \equiv \frac{\sum_{\mu > N/2} \langle |a_\mu(t)|^2 \rangle - \sum_{\mu \leq N/2} \langle |a_\mu(t)|^2 \rangle}{\sum_{\mu=1}^N \langle |a_\mu(t)|^2 \rangle}, \quad (6)$$

where $\langle \cdot \rangle$ denotes the average values of multi-times simulations.

In Fig. 1(a), in the disorder-free case, the oscillations of the imbalance reflect the multiple excitation exchanges between two halves of the chain, and the convergence toward $\mathcal{J} = 0$ demonstrates the delocalization in the absence of disorder. When the disordered strength is applied, in a fully disordered system, the imbalance decreases at a short time, indicating the excitation transport to the left half-chain. The subsequent revival is a result of excitation exchange and dissipation in the left half-chain. By contrast, in a clean-disordered system,

the imbalance converges to a larger value, indicating a less excitation confinement in the clean zone compared to the fully disordered system. As \bar{w} increases, the \mathcal{J} for the clean-disordered case approaches the fully disordered ones, since excitation exchanges are suppressed in both cases.

To further investigate the localization behavior in the right half-chain, in Fig. 1(b) we present the population remaining in the right half-chain as time evolves. In the fully disordered TLQE system, the remaining excitation demonstrates the sustained behaviors in long-time dynamics. In a clean-disordered system, sustained excitation also remains, which demonstrates that delocalization or excitation transport does not dominate the process through spin-exchange interaction with emitters in the clean zone. It indicates the robustness of localization in the disordered zone, even with the presence of emitters in the clean zone which may allow additional excitation loss processes. It appears that the remaining excitation in the clean-disordered system is more than the fully disordered system. However, this property depends on the initial states and interatomic distance ξ . Yet, significant excitation in the clean-disordered system still sustains under different initial states and ξ .

Besides observing the excitation dynamics, the quantum correlation between the clean zone and the disordered zone can also be quantified through the half-chain entropy. With entanglement entropy, the information flow and dissipation in the left half-chain can be identified. The left half-chain entropy is defined as $S_L(t) \equiv \langle \text{Tr} \rho_L(t) \ln \rho_L(t) \rangle$, where $\rho_L(t) \equiv \text{Tr}_R[\rho(t)]$, and $L(R)$ denotes the left (right) part of the array [62]. Given that coherent spin-exchange interaction and collective decay strength in the same order as γ , the time-evolving entropy is mediated by these two factors across all time scales. In Fig. 1(c), the entanglement entropy initially rises with a similar quantity during short-time dynamics for all ranges of disorder strength since short-time dynamics does not engage much of the disorders but deviates after $t \sim \gamma^{-1}$. In the strong disorder regime, the entropy reaches a smaller peak value faster and decreases due to excitation dissipation, indicating the difficulty of information access in the left half-chain for both clean-disordered and fully disordered systems. In comparison, in the disorder-free case, a larger peak value with damping oscillation behavior of the half-chain entropy shows the excitation transport between two half-chains, which indicates the delocalized excitation dynamics. However, in a weaker disorder regime, the competition between interaction and dissipation leads to different behaviors in these setups. For the clean-disordered system, a smaller and earlier entropy peak demonstrates that the decay process dominates in the clean zone when $\gamma t \sim 10^2$. In contrast, a larger and delayed entropy peak represents a more lasting dominance of spin-exchange interaction within this time scale, which leads to the faster loss of excitation transport into the clean zone.

To directly examine the remaining excitation under

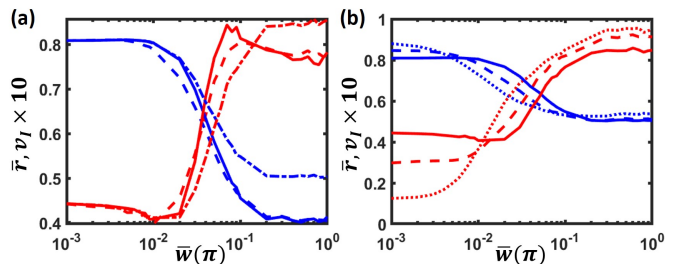


FIG. 2. The mean gap ratio and the intrasample variance with $N = 100$ and $D = 0$ for different disorder strength \bar{w} . (a) At $\xi/\pi = 0.5$, we plot the mean gap ratio (blue line) and intrasample variance (red line) of the fully disordered system (dash line), clean-disordered system (dash-dot line), and the clean-disordered system composed of eigenvalues with more excitation in disordered zone (solid line). (b) The mean gap ratio (blue line) and intrasample variance (red line) of clean-disordered system at $\xi/\pi = 0.125$ (dot), 0.25 (dash), 0.5 (solid).

the influence of the clean zone after long-time evolution, we present the distribution of sustained excitation in the clean-disordered system. In Fig. 1(d), sustained excitation appears in the clean zone near the interface. The non-zero imbalance shown in Fig. 1 (a) also indicates excitation localized in the clean zone. As shown in the inset plot of Fig. 1(d), a larger disorder results in more excitations localized near the interface, while a weaker disorder shows a larger spread for excitation localization, which can be attributed to a balance between the disorder-assisted localization from the disordered zone and the clean-zone-assisted delocalization. The feature that finite excitation localizes at the interface in the clean zone suggests the strong effect as well as the robustness of localization in the disordered zone. From the results in Fig. 1, we find that even though dipole-dipole interaction allows excitation hopping from the disordered zone to the clean zone, the excitation in the disordered zone is still localized as time evolves, which implies the robustness of localization of TLQE system in this parameter regime.

IV. LEVEL STATISTICS AND PARTICIPATION RATIO

To identify the transition from excitation localization to delocalization, we investigate additional measures that help determine the localization crossover, which are level statistics and participation ratio. Level statistics has been extensively applied in studies of quantum chaos [63], which is highly related to the thermalization properties of the system and allows for the classification of them based on the distribution of energy levels. In the tight-binding model of interacting fermions [64, 65], the gap ratio presents Gaussian orthogonal ensemble (GOE) or Poisson statistics (PS) in clean or disordered conditions, respectively. The gap ratio r_j is defined by the ascendant

eigenenergy E_j and the adjacent gaps $\delta_j \equiv E_{j+1} - E_j$, where $r_j \equiv \min\{\delta_j, \delta_{j-1}\}/\max\{\delta_j, \delta_{j-1}\}$ [64]. For each disorder realization, $r_a \equiv \sum_{j=2}^{N-1} r_j/(N-2)$ is defined and the mean gap ratio is obtained by $\bar{r} = \langle r_a \rangle$. A level repulsion in $\bar{r}_{GOE} \approx 0.53$ is presented, compared to $\bar{r}_{PS} \approx 0.39$ with uncorrelated energy levels due to strong disorder. The intrasample variance $v_I \equiv \sum_{n=2}^{N-2} \langle r_n^2 - r_a^2 \rangle$ can also be calculated, which shows the fluctuations of level repulsions [65]. A larger level repulsion indicates the correlation between energy level spacings, which is a crucial feature of the clean system. On the contrary, the disordered system presents a larger intrasample variance with a smaller gap ratio. Through the eigenspectrum of photon-mediated dipole-dipole interaction between each emitter, the level statistics obtained in this TLQE system can provide distinctive features of the localization.

Therefore, via the coupling matrix in Eq. (5), we can extract information from the energy levels of the clean-disordered system. We note that the eigenvalues λ_n are complex due to the non-Hermiticity of the TLQE system, where the real and imaginary parts of eigenvalues correspond to the collective decay rates and energy shifts, respectively. To make sure that the level statistics can be used as a measure for localization crossover, we select the valid sectors of energy levels when the ratio between resonance widths and energy spacings, $(-\text{Re}[\lambda_n + \lambda_{n+1}]/2)/(\text{Im}[\lambda_{n+1} - \lambda_n])$, is less than 1/2 and obtain the gap ratios and intrasample variances. In this way, we can exclude the sectors with superradiant decay rates and retain the eigenspectrum which mostly contains the subradiant sector of decay rates.

In Fig. 2(a), we present the level repulsion and fluctuation at $D = 0$. As the disorder increases, the mean gap ratio decreases and crosses over from delocalization to localization. Based on this, we define the mid-point of the mean gap ratio as the crossover points of disorder strength toward localization. In strong disorder regime, the clean-disordered system exhibits a stronger level repulsion compared to the fully disordered system due to the contribution of the clean zone. This is because the eigenvectors mostly composed of single excitation in the clean zone still contain the feature of a clean system, and therefore these corresponding eigenvalues contribute to a larger mean gap ratio. To examine the feature of \bar{r} in the disordered system, we choose the eigenvector components containing single excitation in the disordered zone more than 0.25 as an additional constraint for selecting eigenvalue sectors. With this constraint, the mean gap ratio and intrasample variance return to the values similar to those of the fully disordered system, indicating the influence of the clean zone on the level statistics, which coincides with the excitation localization in disordered zone shown in Fig. 1(d).

To further study the effect of dipole-dipole interactions on the level statistics, in Fig. 2(b), we show the mean gap ratios and the intrasample variance for different ξ . As ξ increases, the crossover points of disorder strength toward localization shift to a stronger value, which suggests

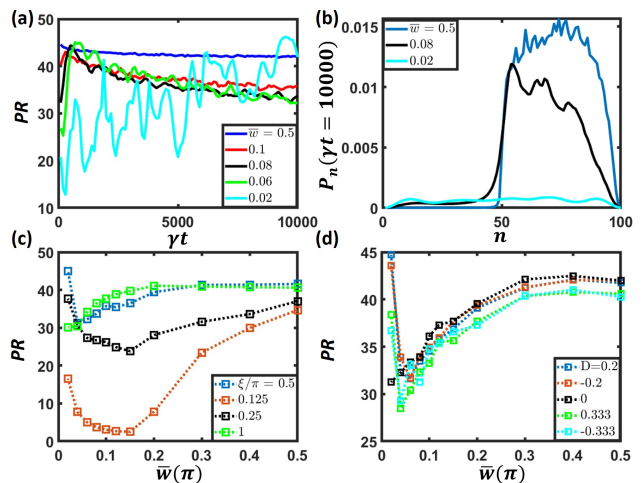


FIG. 3. Participation ratio for $N = 100$ with equal sizes of clean zone and disordered zone. (a) Time evolution of PR for $\xi = 0.5\pi$, $D = 0.2$ under different disorder strength \bar{w} . (b) The excitation distribution for localization with $\bar{w} = 0.5, 0.08$, and 0.02 . The PR (c) for $D = 0.2$ at $\xi/\pi = 0.125, 0.25, 0.5, 1$ and (d) with $\xi = 0.5\pi$ at $D = 0, \pm 0.2, \pm 0.333$ at $\gamma t = 10000$.

a facilitation of the excitation delocalization, similar to the fully disordered case [35]. This can be attributed to the dominance of collective decays at a small ξ and sustained correlations among emitters at a large ξ . The former leads to decoherences of the system and favors the effect of disorders, while the latter indicates a competition between dipole-dipole interactions and disorders, pushing the crossover points toward a stronger disorder strength. We note that at $\xi = 0$ and π in the reciprocal coupling case, decoherence-free states emerge and the localization of atomic excitations sustain indefinitely without disorders.

However, the level statistics can only be utilized in the reciprocal regime. To examine the localization crossover in the non-reciprocal regime ($D \neq 0$), we introduce participation ratio (PR) [66] as a measure to determine the excitation distribution in comparison to the uniform distribution. Since the excitation loss is inherent to the TLQE system, the probability amplitude of the system decreases over time. To focus on the distribution of the remaining excitation, time-dependent PR is defined with $\tilde{P}_\mu(t)$, which represents the onsite probability with the sum normalized to 1

$$\text{PR}(t) \equiv \frac{(\sum_{\mu=1}^N \langle \Delta \tilde{P}_\mu(t) \rangle)^2}{\sum_{\mu=1}^N (\langle \Delta \tilde{P}_\mu(t) \rangle)^2}, \quad (7)$$

where $\Delta \tilde{P}_\mu(t) \equiv |\tilde{P}_\mu(t) - N^{-1}| \Theta(|\tilde{P}_\mu(t) - N^{-1}|)$ with Heaviside function Θ .

As shown in Fig. 3(a), PR is close to the number of quantum emitters in the disordered zone $N/2$ under strong disorders. Owing to the strong localization from the disorders, the probability amplitude is confined in

the disordered zone except at the end. As the disorder strength decreases, PR gradually decreases, which also reflects in the wider excitation spread at the interface shown in Fig. 3(b). We note that PR can serve as a measure for excitation localization when the system is deep in the localization side, but it cannot be used to determine the crossover behavior to localization since it fluctuates over time in the delocalized side.

In Fig. 3(c), we further explore how PR changes under different dipole-dipole interaction strength ξ and directionality D . In strong disorder regime, at $\xi/\pi = 0.125$, a significant decreasing trend of PR occurs as \bar{w} decreases, which demonstrates the tendency of excitation delocalization. On the contrary, at $\xi/\pi = 1$, a less significant decrease of PR occurs as \bar{w} decreases, which represents that the localization is still sustained at a smaller disorder. We observe a similar behavior in PR at $D = 0$, that a smaller ξ facilitating delocalization, which is contrary to the analysis from level statistics in Fig. 2(b). This deviation can be attributed to the initial-state dependence of PR, whereas level statistics in general does not depend on it. In Fig. 3(d), the influences of directionality D are demonstrated. When $D = 0$, PR is larger in the localization side due to the absence of a propagation tendency for the excitation. As D increases, smaller PR reflects a weaker localization since a larger directional coupling strength evades the influence of the disorders [23]. Meanwhile, the trending of PR is similar for the same D with a different sign, demonstrating that the tendency of excitation exchange direction does not modify the localization behavior near the clean-disordered interface even under asymmetric initial states. Even though PR is irregular in the delocalization side, its variation still reflects some features of delocalization in the localization regime in a broad parameter range.

V. DIRECTIONAL PHOTON LOSS RATIO

Besides investigating the localization from the remaining excitation through PR, we study the photon loss from the ends of the TLQE, which can be experimentally measurable by detecting photons dissipation from the ends. Via the input-output theory [67–69], we can illustrate the relationship between the output signal from both ends of the systems and the atomic response. Starting with Hamiltonian including photon basis (Appendix B), the photonic output field is derived as

$$\langle a_{out,d}^\dagger(t) a_{out,d}(t) \rangle = \left\langle \sum_{\mu=1}^N \gamma_d e^{m_d i k(r_\mu - r_\nu)} \sigma_\mu^\dagger(t) \sigma_\nu(t) \right\rangle, \quad (8)$$

where $a_{out,d}^\dagger$ denotes the creation operator of photons leaving the system, with photon propagation direction d such that $m_d = +1(-1)$ for photon toward the left (right). $\gamma_d = \gamma_{L(R)}$ quantifies the strength for left (right)

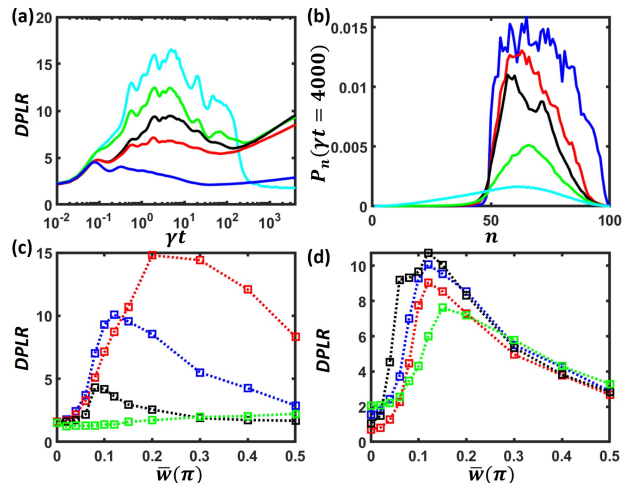


FIG. 4. Directional photon loss ratio for $N = 100$ with equal sizes of clean zone and disordered zone. (a) Time-evolved DPLR and (b) the probability distribution when $\bar{w} = 0.5$ (blue line), 0.2 (red line), 0.15 (black line), 0.1 (green line), 0.02 (cyan line) with $\xi = 0.25\pi, D = 0.2$. (c) DPLR with $D = 0.2$ for $\xi/\pi = 0.125$ (red line), 0.25 (blue line), 0.5 (black line), 1 (green line) at $\gamma t = 4000$. (d) DPLR with $\xi = 0.25\pi$ for $D = -0.2$ (red line), 0 (black line), 0.2 (blue line), 0.333 (green line) at $\gamma t = 4000$.

propagating photon coupling. Besides the collective interaction between emitters, the position of the excitation also determines the loss from the system. If the excitation is close to the left (right) end, then the excitation is more likely to escape from the system as a photon propagating toward the left (right). Therefore, under the asymmetric initial system setup, competing between photon loss from the end and delocalization from the clean-disordered interface can be measured by the directional photon loss ratio (DPLR)

$$\text{DPLR}(t) \equiv \frac{\int_0^t \langle a_{out,R}^\dagger(\tau) a_{out,R}(\tau) \rangle d\tau}{\int_0^t \langle a_{out,L}^\dagger(\tau) a_{out,L}(\tau) \rangle d\tau}. \quad (9)$$

In Fig. 4(a), we show DPLR under different disorder strength \bar{w} with $\xi = 0.25\pi$ as an example. In short-time dynamics, the DPLR rises with a similar quantity for all ranges of disorder strength since the disorders are not engaged in short-time dynamics. However, the evolution of DPLR deviates after $\gamma t \sim 10^{-1}$. In strong disorder regime, the DPLR only slightly decreases until $\gamma t \sim 10^1$ and increases after that. The decrease of DPLR is due to the excitation transport into the clean zone. Once the excitation transport to the clean zone, most of the excitation will exit from the left end of the system, lowering DPLR. After most of the excitation transport into the clean zone is lost, the loss from the sustained excitation in the disordered zone dominates the decay process, resulting in the subsequent revival of DPLR. As a comparison, in a weaker disorder regime, a larger and delayed

peak and subsequent decline of DPLR represent the tendency of delocalization. The former is owing to larger direct loss from the right end, which is also demonstrated in Fig. 4(b), and the latter results from more excitation transport into the clean zone. After $\gamma t \sim 10^2$, in weak disorder regime ($\bar{w} \sim [0.1, 0.2]$), when the localization is still sustained, the excitation transport into the clean zone is limited, resulting in larger DPLR after long-time evolution. On the contrary, when the excitation is delocalized ($\bar{w} \lesssim 0.1$), the excitation can transport into the left half-chain and exits from the left end. Therefore, DPLR decreases and approaches to γ_R/γ_L as the disorder strength decreases to zero in long-time dynamics. Accordingly, we define the localization crossover point of \bar{w} at which the maximal DPLR appears in the long-time regime.

To further investigate the influence of the dipole-dipole interaction strength and directionality D , in Fig. 4(c), we present DPLR under different ξ . The rising and decreasing behavior of DPLR is common when $\xi/\pi = 0.125, 0.25, 0.5$. Larger localization crossover points appear at smaller ξ also indicates the facilitation of delocalization at smaller ξ . However, when $\xi = \pi$, there is no obvious rising or decreasing in DPLR under all ranges of disorder strength. In this case, the initial symmetric Dicke state is close to the decoherence-free state at $D = 0$. Therefore, the excitation dynamics at $\xi = \pi$ is different from the other ξ , and crossover point is hard to be determined in this condition. For the effect of D , in Fig. 4(d), DPLR under different directionality D is presented. In strong disorder regime, the value of DPLR is similar since the excitation dynamics is mainly determined by the disorders. Yet, as \bar{w} decreases, the behavior deviates for different D . The crossover point occurs at a larger \bar{w} when $|D|$ is larger, showing that the excitation localization emerges with a larger disorder strength to counteract the effect of D . In comparison, near the disorder-free regime, the excitation dynamics is mainly determined by directionality D , and DPLR converges to γ_R/γ_L for each D . DPLR serves as an experimental measure for delocalization by utilizing the inherent loss of TLQE systems, which also reflects the complex interplay of disorders, dipole-dipole interaction, and directionality. We note that the photon loss also depends on the initial state. Therefore, different initial states result in different behaviors of the DPLR.

VI. SIZE EFFECTS

Finally, we search for the signature of quantum avalanche-like behaviors in the TLQE system through investigating the size effects on the clean-disordered interface via the mean gap ratio, PR, and DPLR. The size of the clean zone plays a crucial role in determining quantum avalanche dynamics in many-body localization system [18], where a larger clean zone size leads to a faster delocalization from the clean-disordered interface.

Therefore, we explore the delocalization phenomenon in a similar fashion by modifying the relative sizes between the clean and the disordered zones. In Fig. 5, we present several cases of different size parameters. The first case is to change the overall size of the TLQE systems with a fixed ratio of clean zone. The results are shown in Fig. 5(a). As the overall system size increases, the phase crossover points measured by the mean gap ratio occur at smaller disorder strength \bar{w} , which demonstrates the enhancement of localization via scaling. In addition, Figs. 5(b) and 5(c) present that the value of PR/N_d decreases slower as \bar{w} decreases in the strong disorder regime, where $N_d(N_c)$ denotes the atomic number in the disordered (clean) zone. It indicates that the robustness of the localization is also enhanced in a larger system. Meanwhile, DPLR in Fig. 5(d) shows that the localization crossover points and the photon scattering behavior is saturated as size increases, which indicates that the system reaches a thermodynamic limit of scaling. Both PR/N_d and DPLR provide insights into the finite size effects on the clean-disordered interface and the influence of direct loss at the end of the system.

The second case is to investigate the effect of tuning the ratio of the clean-disordered zone on the phase crossover of excitation localization. As shown in Fig. 5(e), as the ratio of the clean zone increases, the phase crossover points determined by the mean gap ratio occur at larger disorder strength \bar{w} , which demonstrates that the ratio of the clean zone facilitate the excitation delocalization. In Fig. 5(f), PR over the atomic number in disordered zone N_d is presented for different clean-disordered zone size ratios when $N = 500$. We find that as the ratio of clean zone increases, the value of PR/N_d decreases faster as \bar{w} decreases in the strong disorder regime. We note that when N_d is close to N , the excitation distribution will be close to the uniform distribution. Therefore, PR is inaccurate in this parameter regime since PR involves a comparison of excitation distribution to the uniform distribution. The results shown in Figs. 5(e) and 5(f) represent the enhancement of excitation delocalization as the ratio of clean zone increases. In other words, as the ratio of disordered zone increases, the excitation localization is favored. On the other hand, as the overall size of the system increases with a fixed ratio, the excitation localization is favored for a smaller disorder strength owing to the multi-atom effect on the suppression of spin hoppings.

In the end, we follow the analysis in the experimental work [18] by tuning the number of emitters in the clean zone N_c while keeping the number of emitters in the disordered zone N_d constant. As shown in Fig. 5(g), in strong disorder regime, when $N_c < 20$, PR decreases more significantly as the disorder strength \bar{w} decreases due to the boundary loss from the left end. In contrast, when the clean zone size is large enough, PR converges to a constant value in the strong disorder regime, which reflects the excitation localization in the disordered zone at the interface. Meanwhile, in Fig. 5(h),

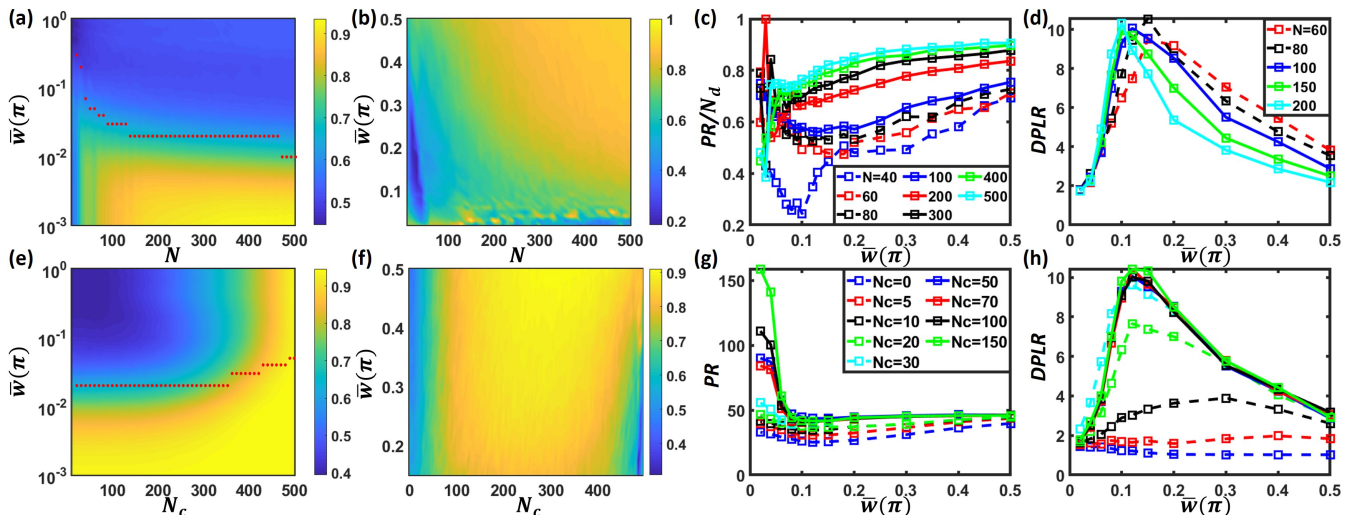


FIG. 5. The mean gap ratio, PR and DPLR under different sizes and clean-disordered zone ratios. (a) The mean gap ratio under $D = 0$, (b) PR/N_d under $D = 0.2, \gamma t = 4000$ with different quantum emitter numbers and \bar{w} for $\xi = 0.25\pi$ and $N_c = N_d$. (c) PR/N_d with different N in (b). (d) DPLR for $N = 50, 100, 150, 200$ under different disorder strength with equal size in clean order zone and disordered zone size. (e) The mean gap ratio with $D = 0$ (f) PR with $D = 0.2, \gamma t = 4000$ varies N_c and \bar{w} while $N = 500$ and $\xi = 0.25\pi$. (g)(h) PR and DPLR with different size of clean zone while $N_d = 50, \xi = 0.25\pi, D = 0.2, \gamma t = 4000$. The red dots in (a) and (e) represents the localization crossover points.

when $N_c < 20$, DPLR remains almost constant under every disorder strength because of excitation loss from both ends of the TLQE system. Whereas once $N_c \geq 20$, the phase crossover points determined by DPLR becomes constant, and the rising and declining features of DPLR are recovered, which demonstrates the convergence of collective dissipation behaviors once the boundary loss from the left end is not dominated. These suggest that the effect of overall size on enhancing the localization is more significant than the effect of the clean zone ratio that facilitates delocalization under a fixed number of the whole chain.

VII. DISCUSSION

The absence of delocalization enhancement in the TLQE system demonstrates a fundamental difference in localization mechanisms compared to other systems. In TLQE system, the position fluctuations of the emitters result in a random and complex spin-exchange process between each emitter, which leads to excitation localization. Under this disorder-assisted localization, the excitations still redistribute through the coherent hoppings and collective decay as time evolves. From the analysis of level statistics, we find that while TLQE exhibits level repulsion under weak disorder, larger mean gap ratio appears in clean-disordered system under strong disorder regime compared to fully disordered system due to the contribution of the clean zone. We further calculate the participation ratio which can quantify the distribution of excitations and localization behaviors. In addition, the

directional photon loss ratio also reflects the localization behaviors. When the excitations are delocalized, the excitations spread through the whole chain and decay from both sides, resulting in the declining feature of DPLR in the delocalized side. Therefore, we utilize the maximal point of DPLR as a measure of localization crossover points. With these measures, how the localization behaviors influenced by the scaling size can be determined. A larger disordered zone leads to the tendency of localization, whereas increasing the size of the clean zone does not enhance delocalization. This can also be interpreted as that the scaling overall size that enhances localization surpasses the effect from the clean zone ratio that facilitates the delocalization with a fixed overall size.

There are several potential platforms to experimentally observe the excitation dynamics in the clean-disordered system and detect the directional photon loss. One potential platform is atoms coupled to an optical fiber [31, 70–73]. In recent experiments [31, 70–73], hundreds of cesium atoms can be confined surrounding an optical fiber via the evanescent field of the guided mode. Dipole-dipole interaction between atoms are mediated by the guided photons in the fibers and give rise to strong collective interaction behaviors. If photon detectors are attached at the ends of the optical fiber, radiative photon loss can be further detected. An alternative approach to observe the localization to delocalization crossover can be done by directly detecting excitation population. Through shining the laser with proper transition frequencies from the side, the excitation can be detected. This method is widely used in ultracold atom experiments for quantum state detection. Another potential platform is superconducting qubits, in which many-body localization

has already been experimentally explored [74, 75]. With the cavity, microwave photons emitted from superconducting qubits can be captured and observed [76–78].

Beyond the scope of this work, we propose other potential future research directions. For example, we can extend to multiple excitations regime for investigating how many-body effects influence current results in this unique system. Very recently, many-body localization in waveguide QED has been explored [28, 29]. Further exploration with input fields on the current system can provide more insights on the excitation dynamics. Another potential work is to decompose an atomic chain into several chains with different interatomic distances. With the excitation transport to the interface between these dissimilar chains, one can study the excitation transmission and reflection resulting from the collective interactions among the emitters.

ACKNOWLEDGMENTS

We acknowledge support from the National Science and Technology Council (NSTC), Taiwan, under Grants No. 112-2112-M-001-079-MY3, No. NSTC-112-2119-M-001-007, No. 112-2811-M-002-067, and No. 112-2112-M-002-001. We are also grateful for support from TG 1.2 of NCTS at NTU.

Appendix A: Resonant dipole-dipole interaction in one-dimensional reservoir

We consider an emitter arrays coupled to a waveguide which offers a common 1D reservoir [53, 60, 79]. For the μ -th two-level emitter, we denote $|e\rangle_\mu$ and $|g\rangle_\mu$ for the excited and ground states with transition frequency ω_{eg} . The system Hamiltonian H_{sys} reads,

$$H_{sys} = \hbar \sum_{\mu=1}^N \omega_{eg} \sigma_\mu^\dagger \sigma_\mu^-, \quad (\text{A1})$$

where $\sigma_\mu^\dagger \equiv |e\rangle_\mu \langle g|$ with $\sigma_\mu = (\sigma_\mu^\dagger)^\dagger$ denotes the dipole operator.

The corresponding reservoir Hamiltonian H_r reads

$$H_r = \sum_q \sum_{d=L,R} \hbar \omega_{\omega_q,d} a_{\omega_q,d}^\dagger a_{\omega_q,d}, \quad (\text{A2})$$

where $a_{\omega_q,d}$ are bosonic annihilation operators for the right (left) propagating bath modes q with frequency ω_q for $d = R(L)$.

In the interaction picture, the system-reservoir interaction is given by

$$H_{sys-r} = i\hbar \sum_{\mu,d,q} g_{\omega_q,d} (\sigma_\mu^\dagger + \sigma_\mu) (a_{\omega_q,d}^\dagger e^{i(\omega_q t - \omega x_\mu / v_d)} + a_{\omega_q,d} e^{-i(\omega_q t - \omega x_\mu / v_d)}), \quad (\text{A3})$$

where $g_L(g_R)$ is the emitter-photon coupling strength into the left(right) propagating reservoir modes with speed v_d .

Therefore, the reservoir operators $a_{\omega_q,d}(t)$ can be obtained by solving the Heisenberg equations of motion

$$a_{\omega_q,d}(t) = a_{\omega_q,d}(0) e^{-i\omega t} + i \int_0^t dt' \sum_{\mu=1}^N g_{\omega_q,d} [\sigma_\mu(0) + \sigma_\mu^\dagger(0)] e^{-i\omega_q t'} e^{-i\omega_q x_\mu / v_d}. \quad (\text{A4})$$

For an arbitrary emitter operator A acting on the Hilbert space of the spins, we obtain

$$\dot{A}(t) = i\omega_{eg} \sum_{\mu} [\sigma_\mu^\dagger \sigma_\mu, A] - i \sum_{\mu,d,q} g_{\omega_q,d} \{ e^{ik_{d,q} x_\mu} [\sigma_\mu^\dagger + \sigma_\mu, A] a_{\omega_q,d}(t) + e^{-ik_{d,q} x_\mu} a_{\omega_q,d}^\dagger(t) [A, \sigma_\mu^\dagger + \sigma_\mu] \},$$

where $k_{d,q} \equiv \omega_q / v_d$. We assume Born-Markov approximation is valid in our system. The Born approximation states that the coupling between the emitters and the reservoir modes is so weak that the system operators can be approximately related to the first order of the coupling strength. Markov approximation suggests that the correlation time between the bath and the system is so short compared to the system evolution. Besides, we neglect the time retardation effect from photon propagation, which is valid when the time scales of system operators evolution is much larger than the time for photon propagation in the waveguide. The initial bath state is assumed to be the vacuum state. We then obtain the expectation value of system operator $\langle A(t) \rangle = \text{Tr}\{A(t)W(0)\}$ by tracing over the reservoir modes, where $W(0)$ is the density matrix of the initial system $= \rho(0) \otimes |vac\rangle \langle vac|$. The equation of motion $\langle A(t) \rangle$ is given by

$$\langle \dot{A} \rangle(t) = \sum_{\mu \neq \nu, d} i\Omega_{\mu,\nu,d} [\sigma_\mu^\dagger \sigma_\nu, A] + \sum_d \mathcal{L}_d(A), \quad (\text{A5})$$

where

$$\mathcal{L}_d(A) = \sum_{\mu,\nu} \Gamma_{\mu,\nu,d} [\sigma_\mu^\dagger A \sigma_\nu - \frac{1}{2} (A \sigma_\mu^\dagger \sigma_\nu + \sigma_\mu^\dagger \sigma_\nu A)]. \quad (\text{A6})$$

The coupling strength $J_{\mu,\nu,d} \equiv \frac{1}{2} \Gamma_{\mu,\nu,d} + i\Omega_{\mu,\nu,d}$ can be obtained as

$$\begin{aligned}
J_{\mu,\nu,d} &= \sum_q \int_0^t ds |g_{\omega_q,d}|^2 e^{ik_{d,q}x_{\mu,\nu}} (e^{i(\omega_{eg}-\omega)s} + e^{-i(\omega_{eg}+\omega)s}) \\
&= \sum_q |g_{\omega_q,d}|^2 e^{ik_{d,q}x_{\mu,\nu}} [\pi\delta(\omega_{eg}-\omega) + \pi\delta(\omega_{eg}+\omega) \\
&\quad + i\mathcal{P}(\omega_{eg}-\omega)^{-1} - i\mathcal{P}(\omega_{eg}+\omega)^{-1}],
\end{aligned}$$

where \mathcal{P} denotes the principal values, and $x_{\mu,\nu} \equiv x_\mu - x_\nu$.

Considering the summation of the mode to the continuous limit, $\Sigma_q \rightarrow \int \frac{dq}{2\pi} L$, where L is the quantization length.

Therefore, we have

$$\begin{aligned}
J_{\mu,\nu,d} &= \int_0^\infty \frac{dq}{2\pi} \bar{g}_{\omega_q,d}^2 L e^{ik_{\omega,d}x_{\mu,\nu}} [\pi\delta(\omega_{eg}-\omega) \\
&\quad + \pi\delta(\omega_{eg}+\omega) + i\mathcal{P}(\omega_{eg}-\omega)^{-1} - i\mathcal{P}(\omega_{eg}+\omega)^{-1}] \\
&= \int_0^\infty \frac{d\omega}{2\pi} |\partial_\omega q(\omega)| \bar{g}_{\omega_q,d}^2 L e^{ik_{\omega,d}x_{\mu,\nu}} [\pi\delta(\omega_{eg}-\omega) \\
&\quad + \pi\delta(\omega_{eg}+\omega) + i\mathcal{P}(\omega_{eg}-\omega)^{-1} - i\mathcal{P}(\omega_{eg}+\omega)^{-1}] \\
&= \int_0^\infty \frac{d\omega}{4\pi} \gamma_d e^{ik_{\omega,d}x_{\mu,\nu}} [\pi\delta(\omega_{eg}-\omega) \\
&\quad + \pi\delta(\omega_{eg}+\omega) + i\mathcal{P}(\omega_{eg}-\omega)^{-1} - i\mathcal{P}(\omega_{eg}+\omega)^{-1}].
\end{aligned}$$

where $\gamma_d \equiv 2|\partial_\omega q(\omega)| \bar{g}_{\omega_q,d}^2 L$ and $k_{\omega,d} \equiv \omega/v_d$.

Finally, we simplify the equation above as

$$\begin{aligned}
J_{\mu,\nu,d} &= \frac{\gamma_d}{4} e^{ik_{\omega,d}x_{\mu,\nu}} - i \frac{\mathcal{P}}{2\pi} \int d\omega \frac{\gamma_d e^{ik_{\omega,d}x_{\mu,\nu}}}{\omega - \omega_{eg}}, \\
&= \frac{\gamma_d}{4} e^{ik_{\omega,d}x_{\mu,\nu}} + i \frac{\gamma_d}{4} \sin(|k_{\omega,d}x_{\mu,\nu}|). \quad (\text{A7})
\end{aligned}$$

This coupling strength $J_{\mu,\nu,d}$ provides the foundation of the chiral coupling in Eqs.(1) to Eqs.(3).

Appendix B: Photon Flux

To observe the photon flux propagating out the system, instead of using the master equation and effective Hamiltonian [52] which traces out the photonic fields, we consider the Hamiltonian including both atomic and photonic basis. Therefore, the Hamiltonian of this system H can be decomposed of the emitter term H_{em} , photonic terms H_p , and emitter-photon interaction terms H_{em-p} :

$$H = H_{em} + H_p + H_{em-p}, \quad (\text{B1})$$

where

$$H_{em} = \sum_\mu \hbar\omega_{eg} \sigma_\mu^\dagger \sigma_\mu^- \quad (\text{B2})$$

$$H_p = \sum_d \int \hbar\omega a_{\omega,d}^\dagger a_{\omega,d} d\omega \quad (\text{B3})$$

$$H_{em-p} = i\hbar \sum_{\mu,d} \int d\omega (g_d e^{m_d i k_s x_\mu}) \sigma_\mu a_{\omega,d}^\dagger + \text{H.c.}, \quad (\text{B4})$$

where k_s and g_d denote the photon wave vector and the coupling constant between quantum emitters. The photon with propagation direction d toward the left (right) such that $m_d = +1(-1)$. $a_{\omega,d} (a_{\omega,d}^\dagger)$ denotes the annihilation (creation) operator of the photon with frequency ω and direction d .

To obtain the output photon flux, we calculate the annihilation operator in Heisenberg picture.

$$\begin{aligned}
\frac{da_{\omega,d}}{dt} &= \frac{i}{\hbar} [H, a_{\omega,d}] \\
&= -i\omega a_{\omega,d} - \sum_\mu (g_d e^{m_d i k_s x_\mu}) \sigma_\mu, \quad (\text{B5})
\end{aligned}$$

after integrating to time, we have annihilation operator

$$\begin{aligned}
a_{\omega,d}(t) &= a_{\omega,d}(t_0) e^{-i\omega(t-t_0)} \\
&\quad - \int_{t_0}^t ds \sum_\mu (g_d e^{m_d i k_s x_\mu}) \sigma_\mu e^{-i\omega(t-s)}
\end{aligned}$$

and

$$\begin{aligned}
a_{\omega,d}(t) &= a_{\omega,d}(t_f) e^{-i\omega(t-t_f)} \\
&\quad - \int_{t_f}^t ds \sum_\mu (g_d e^{m_d i k_s x_\mu}) \sigma_\mu e^{-i\omega(t-s)},
\end{aligned}$$

where we set our initial condition of the time integral as initial time t_0 and final time t_f .

Therefore, we have

$$\begin{aligned}
a_{\omega,d}(t_f) e^{-i\omega(t-t_f)} &= a_{\omega,d}(t_0) e^{-i\omega(t-t_0)} \\
&\quad + \int_{t_0}^{t_f} ds \sum_\mu (g_d e^{m_d i k_s x_\mu}) \sigma_\mu e^{-i\omega(t-s)}. \quad (\text{B6})
\end{aligned}$$

Integrating over the frequency ω , we have

$$\begin{aligned}
&\int d\omega a_{\omega,d}(t_f) e^{-i\omega(t-t_f)} \\
&= \int d\omega a_{\omega,d}(t_0) e^{-i\omega(t-t_0)} + \int d\omega \int_{t_0}^{t_f} ds \\
&\quad \sum_\mu (g_d e^{m_d i k_s x_\mu}) \sigma_\mu e^{-i\omega(t-s)}.
\end{aligned}$$

Defining the output signal operator $a_{out,d}(t)$ and the input signal operator $a_{in,d}(t)$ as

$$a_{out,d}(t) \equiv \frac{1}{\sqrt{2\pi}} \int d\omega a_{\omega,d}(t_f) e^{-i\omega(t-t_f)},$$

and

$$a_{in,d}(t) \equiv \frac{1}{\sqrt{2\pi}} \int d\omega a_{\omega,d}(t_0) e^{-i\omega(t-t_0)}.$$

The input-output relation is obtained as

$$a_{out,d}(t) = a_{in,d}(t) + \sqrt{2\pi} \sum_{\mu} (g_d e^{m_d i k_s x_{\mu}}) \sigma_{\mu}(t).$$

In our system setup, there is no photonic input source for driving atomic transitions. Therefore, $a_{in}(t) = 0$, and

$$a_{out,d}(t) = \sqrt{2\pi} \sum_{\mu} (g_d e^{m_d i k_s x_{\mu}}) \sigma_{\mu}(t). \quad (\text{B7})$$

With defining $\gamma_d \equiv 2\pi g_d^2$, then output photon flux is obtained as

$$\langle a_{out,d}^{\dagger}(t) a_{out,d}(t) \rangle = \langle \sum_{\mu,\nu} \gamma_d e^{m_d i k_s (x_{\mu} - x_{\nu})} \sigma_{\mu}^{\dagger}(t) \sigma_{\nu}(t) \rangle, \quad (\text{B8})$$

where $m_d = +1(-1)$ for the left (right) propagation. $\gamma_d = \gamma_{L(R)}$ when photonic propagation direction d is toward the left (right).

-
- [1] P. W. Anderson, *Physical Review* **109**, 1492 (1958).
 - [2] F. Jendrzejewski, A. Bernard, K. Müller, P. Cheinet, V. Josse, M. Piraud, L. Pezzé, L. Sanchez-Palencia, A. Aspect, and P. Bouyer, *Nature Physics* **8**, 398 (2012).
 - [3] T. S. Tsoi and C. K. Law, *Physical Review A* **78**, 063832 (2008).
 - [4] S. S. Kondov, W. R. McGehee, J. J. Zirbel, and B. Demarco, *Science* **334**, 66 (2011).
 - [5] Y. Lahini, A. Avidan, F. Pozzi, M. Sorel, R. Morandotti, D. N. Christodoulides, and Y. Silberberg, *Physical Review Letters* **100**, 013906 (2008).
 - [6] T. Schwartz, G. Bartal, S. Fishman, and M. Segev, *Nature* **446**, 52 (2007).
 - [7] F. Evers and A. D. Mirlin, *Reviews of Modern Physics* **80**, 1355 (2008).
 - [8] D. Clément, A. F. Varón, M. Hugbart, J. A. Retter, P. Bouyer, L. Sanchez-Palencia, D. M. Gangardt, G. V. Shlyapnikov, and A. Aspect, *Physical Review Letters* **95**, 170409 (2005).
 - [9] P. Schmitteckert, T. Schulze, C. Schuster, P. Schwab, and U. Eckern, *Physical Review Letters* **80**, 560 (1998).
 - [10] T. Paul, M. Albert, P. Schlagheck, P. Leboeuf, and N. Pavloff, *Physical Review A* **80**, 033615 (2009).
 - [11] P. Sierant and J. Zakrzewski, *Physical Review B* **105**, 224203 (2022).
 - [12] Y. B. Lev and D. R. Reichman, *Physical Review B* **89**, 220201 (2014).
 - [13] M. Serbyn, D. A. Abanin, and Z. Papić, *Nature Physics* **17**, 675 (2021).
 - [14] J. P. Eckmann and D. Ruelle, *Reviews of Modern Physics* **57**, 617 (1985).
 - [15] C. J. Turner, A. A. Michailidis, D. A. Abanin, M. Serbyn, and Z. Papić, *Nature Physics* **14**, 745 (2018).
 - [16] D. Sels, *Physical Review B* **106**, 1020202 (2022).
 - [17] D. J. Luitz, F. Huveneers, and W. D. Roeck, *Physical Review Letters* **119**, 150602 (2017).
 - [18] J. Léonard, S. Kim, M. Rispoli, A. Lukin, R. Schittko, J. Kwan, E. Demler, D. Sels, and M. Greiner, *Nature Physics* **19**, 481 (2023).
 - [19] A. Morningstar, L. Colmenarez, V. Khemani, D. J. Luitz, and D. A. Huse, *Physical Review B* **105**, 174205 (2022).
 - [20] W. D. Roeck and F. Huveneers, *Physical Review B* **95**, 155129 (2017).
 - [21] T. Thiery, F. Huveneers, M. Müller, and W. D. Roeck, *Physical Review Letters* **121**, 140601 (2018).
 - [22] N. Fayard, L. Henriot, A. Asenjo-Garcia, and D. E. Chang, *Physical Review Research* **3**, 033233 (2021).
 - [23] H. H. Jen, *Physical Review A* **102**, 043525 (2020).
 - [24] H. P. Lüschen, P. Bordia, S. S. Hodgman, M. Schreiber, S. Sarkar, A. J. Daley, M. H. Fischer, E. Altman, I. Bloch, and U. Schneider, *Physical Review X* **7**, 011034 (2017).
 - [25] D. Roy, C. Wilson, and O. Firstenberg, *Reviews of Modern Physics* **89**, 021001 (2017).
 - [26] A. S. Sheremet, M. I. Petrov, I. V. Iorsh, A. V. Poshakinskiy, and A. N. Poddubny, *Reviews of Modern Physics* **95**, 015002 (2023).
 - [27] K. Y. Bliokh and F. Nori, *Physics Reports* **592**, 1 (2015).
 - [28] P. Manasi and D. Roy, *Physical Review A* **98**, 023802 (2018).
 - [29] T. F. See, V. M. Bastidas, J. Tangpanitanon, and D. G. Angelakis, *Physical Review A* **99**, 033835 (2019).
 - [30] J. D. Hood, A. Goban, A. Asenjo-Garcia, M. Lu, S.-P. Yu, D. E. Chang, and H. J. Kimble, *Proceedings of the National Academy of Sciences* **113**, 10507 (2016).
 - [31] P. Solano, P. Barberis-Blostein, F. K. Fatemi, L. A. Orozco, and S. L. Rolston, *Nature Communications* **8**, 10.1038/s41467-017-01994-3 (2017).
 - [32] A. Tiranov, V. Angelopoulou, C. J. van Diepen, B. Schirnski, O. A. D. Sandberg, Y. Wang, L. Midolo, S. Scholz, A. D. Wieck, A. Ludwig, A. S. Sørensen, and P. Lodahl, *Science* **379**, 389 (2023).
 - [33] N. Defenu, T. Donner, T. Macrì, G. Pagano, S. Ruffo, and A. Trombettoni, *Reviews of Modern Physics* **95**, 035002 (2023).
 - [34] S. Mahmoodian, G. Calajó, D. E. Chang, K. Hammerer, and A. S. Sørensen, *Physical Review X* **10**, 031011 (2020).
 - [35] H. H. Jen and J.-S. You, *Journal of Physics B: Atomic, Molecular and Optical Physics* **54**, 105002 (2021).
 - [36] I. M. Mirza, J. G. Hoskins, and J. C. Schotland, *Physical Review A* **96**, 053804 (2017).

- [37] H. H. Jen, *Physical Review A* **105**, 023717 (2022).
- [38] S. Mahmoodian, M. Čepulkovskis, S. Das, P. Lodahl, K. Hammerer, and A. S. Sørensen, *Physical Review Letters* **121**, 143601 (2018).
- [39] Z. Liao, X. Zeng, S.-Y. Zhu, and M. S. Zubairy, *Physical Review A* **92**, 023806 (2015).
- [40] G.-Z. Song, E. Munro, W. Nie, L.-C. Kwek, F.-G. Deng, and G.-L. Long, *Physical Review A* **98**, 023814 (2018).
- [41] R. Gutiérrez-Jáuregui and A. Asenjo-Garcia, *Physical Review Research* **4**, 013080 (2022).
- [42] S. J. Masson and A. Asenjo-Garcia, *Physical Review Research* **2**, 043213 (2020).
- [43] H. H. Jen, M.-S. Chang, and Y.-C. Chen, *Physical Review A* **94**, 013803 (2016).
- [44] H. H. Jen, *Physical Review A* **96**, 023814 (2017).
- [45] J. A. Needham, I. Lesanovsky, and B. Olmos, *New Journal of Physics* **21**, 073061 (2019).
- [46] H. H. Jen, *Physical Review A* **103**, 063711 (2021).
- [47] J. S. Douglas, H. Habibian, C.-L. Hung, A. V. Gorshkov, H. J. Kimble, and D. E. Chang, *Nature Photonics* **9**, 326 (2015).
- [48] L. Henriët, J. S. Douglas, D. E. Chang, and A. Albrecht, *Physical Review A* **99**, 023802 (2019).
- [49] H. H. Jen, *Journal of Physics B: Atomic, Molecular and Optical Physics* **52**, 065502 (2019).
- [50] J. Zhong, N. A. Olekhno, Y. Ke, A. V. Poshakinskiy, C. Lee, Y. S. Kivshar, and A. N. Poddubny, *Physical Review Letters* **124**, 093604 (2020).
- [51] P. Lodahl, S. Mahmoodian, S. Stobbe, A. Rauschenbeutel, P. Schneeweiss, J. Volz, H. Pichler, and P. Zoller, *Nature* **541**, 473 (2017).
- [52] H. Pichler, T. Ramos, A. J. Daley, and P. Zoller, *Physical Review A* **91**, 042116 (2015).
- [53] R. H. Lehmberg, *Physical Review A* **2**, 883 (1970).
- [54] R. H. Dicke, *Physical Review* **93**, 99 (1954).
- [55] K. Y. Bliokh, F. J. Rodríguez-Fortuño, F. Nori, and A. V. Zayats, *Nature Photonics* **9**, 796 (2015).
- [56] M. Scheucher, A. Hilico, E. Will, J. Volz, and A. Rauschenbeutel, *Science* **354**, 1577 (2016).
- [57] J. Petersen, J. Volz, and A. Rauschenbeutel, *Science* **346**, 67 (2014).
- [58] I. Söllner, S. Mahmoodian, S. L. Hansen, L. Midolo, A. Javadi, G. Kiršanské, T. Pregnolato, H. El-Ella, E. H. Lee, J. D. Song, S. Stobbe, and P. Lodahl, *Nature Nanotechnology* **10**, 775 (2015).
- [59] R. Mitsch, C. Sayrin, B. Albrecht, P. Schneeweiss, and A. Rauschenbeutel, *Nature Communications* **5**, 10.1038/ncomms6713 (2014).
- [60] A. González-Tudela and D. Porras, *Physical Review Letters* **110**, 080502 (2013).
- [61] K. Stannigel, P. Rabl, and P. Zoller, *New Journal of Physics* **14**, 063014 (2012).
- [62] J. H. Bardarson, F. Pollmann, and J. E. Moore, *Physical Review Letters* **109**, 017202 (2012).
- [63] D. A. Abanin, E. Altman, I. Bloch, and M. Serbyn, *Reviews of Modern Physics* **91**, 021001 (2019).
- [64] V. Oganesyan and D. A. Huse, *Physical Review B* **75**, 155111 (2007).
- [65] P. Sierant and J. Zakrzewski, *Physical Review B* **99**, 104205 (2019).
- [66] N. C. Murphy, R. Wortis, and W. A. Atkinson, *Physical Review B* **83**, 184206 (2011).
- [67] M. J. Collett and C. W. Gardiner, *Physical Review A* **30**, 1386 (1984).
- [68] C. W. Gardiner and M. J. Collett, *Physical Review A* **31**, 3761 (1985).
- [69] K. Lalumière, B. C. Sanders, A. F. van Loo, A. Fedorov, A. Wallraff, and A. Blais, *Physical Review A* **88**, 043806 (2013).
- [70] N. V. Corzo, J. Raskop, A. Chandra, A. S. Sheremet, B. Gouraud, and J. Laurat, *Nature* **566**, 359 (2019).
- [71] A. S. Prasad, J. Hinney, S. Mahmoodian, K. Hammerer, S. Rind, P. Schneeweiss, A. S. Sørensen, J. Volz, and A. Rauschenbeutel, *Nature Photonics* **14**, 719 (2020).
- [72] P. Solano, J. A. Grover, J. E. Hoffman, S. Ravets, F. K. Fatemi, L. A. Orozco, and S. L. Rolston, *Optical nanofibers*, in *Advances In Atomic, Molecular, and Optical Physics* (Elsevier, 2017) pp. 439–505.
- [73] C. Sayrin, C. Junge, R. Mitsch, B. Albrecht, D. O’Shea, P. Schneeweiss, J. Volz, and A. Rauschenbeutel, *Physical Review X* **5**, 041036 (2015).
- [74] P. Roushan, C. Neill, J. Tangpanitanon, V. M. Bastidas, A. Megrant, R. Barends, Y. Chen, Z. Chen, B. Chiaro, A. Dunsworth, A. Fowler, B. Foxen, M. Giustina, E. Jeffrey, J. Kelly, E. Lucero, J. Mutus, M. Neeley, C. Quintana, D. Sank, A. Vainsencher, J. Wenner, T. White, H. Neven, D. G. Angelakis, and J. Martinis, *Science* **358**, 1175 (2017).
- [75] K. Xu, J.-J. Chen, Y. Zeng, Y.-R. Zhang, C. Song, W. Liu, Q. Guo, P. Zhang, D. Xu, H. Deng, K. Huang, H. Wang, X. Zhu, D. Zheng, and H. Fan, *Physical Review Letters* **120**, 050507 (2018).
- [76] Y. Lu, A. Bengtsson, J. J. Burnett, E. Wiegand, B. Suri, P. Krantz, A. F. Roudsari, A. F. Kockum, S. Gasparinetti, G. Johansson, and P. Delsing, *npj Quantum Inf.* **7**, 10.1038/s41534-021-00367-5 (2021).
- [77] F. Helmer, M. Mariani, E. Solano, and F. Marquardt, *Physical Review A* **79**, 052115 (2009).
- [78] B. R. Johnson, M. D. Reed, A. A. Houck, D. I. Schuster, L. S. Bishop, E. Ginossar, J. M. Gambetta, L. DiCarlo, L. Frunzio, S. M. Girvin, and R. J. Schoelkopf, *Nature Physics* **6**, 663 (2010).
- [79] H. H. Jen, M.-S. Chang, G.-D. Lin, and Y.-C. Chen, *Physical Review A* **101**, 023830 (2020).